Higher harmonics of the *ac* susceptibility: Analysis of hysteresis effects in ultrathin ferromagnets

C. Rüdt,* P. J. Jensen, A. Scherz, J. Lindner, P. Poulopoulos,† and K. Baberschke
Physics Department, Freie Universität Berlin, Arnimallee 14, D-14195 Berlin, Germany
(Received 22 July 2003; revised manuscript received 13 October 2003; published 28 January 2004)

The initial *ac* susceptibility is used to monitor the higher harmonic susceptibilities $\chi_n(T,\omega_0)$ as a function of temperature. To our knowledge, for the first time we present $\chi_n(T,\omega_0)$ up to $n=11$ for a $(Fe_2/V_5)_{50}$ superlattice in the ultrathin-film limit. A detailed analysis of $\chi_n(T,\omega_0)$ yields the full temperature-dependent hysteresis loops, including the coercive field $H_C(T)$ and the saturation magnetization $M_S(T)$, with high accuracy close to the Curie temperature T_C. We show that this type of analysis allows for an independent determination of T_C. In addition, the $\chi_n(T,\omega_0)$ are calculated in the framework of a mean-field theory which compares well with the experimental data.

DOI: 10.1103/PhysRevB.69.014419 PACS number(s): 75.40.Cx, 68.35.Rh, 73.21.Cd

I. INTRODUCTION

Direct measurements of the magnetization $M(T)$ which vanishes at the Curie temperature T_C are only sensitive to the expectation value $\langle S^z\rangle$. In contrast, the paramagnetic susceptibility $\chi_{pm}(T)$ is superior due to its proportionality to $\langle S^2\rangle$ and its divergence on both sides of the paramagnetic to ferromagnetic second-order phase transition according to[1]

$$\chi_{pm}(\varepsilon)=\chi_0^{\pm}|\varepsilon|^{-\gamma}. \tag{1}$$

$\chi_0^{\pm}$ is the critical amplitude below and above T_C, $\varepsilon=(T-T_C)/T_C$ the reduced temperature, and γ the critical exponent. The measurement of the susceptibility is a powerful tool to accurately determine T_C and has been extensively used in the past.[2–6] Nevertheless, the simultaneous determination of all critical parameters T_C, γ, and $\chi_0^{\pm}$, Eq. (1), leads to difficulties.

In this paper we show that an alternative method to determine T_C independent of Eq. (1) is provided by the measurement and analysis of higher harmonics $\chi_n(T,\omega_0)$. Little work investigating these $\chi_n(T,\omega_0)$ has been reported in the past.[7–10] For instance, Carré and Souletie[10] predicted that the coefficients $\chi_n(T,\omega_0)=\chi_n'(T,\omega_0)+i\chi_n''(T,\omega_0)$ of order n exhibit universal power laws corresponding to Eq. (1) with critical parameters γ_n and $\chi_{0,n}^{\pm}$, where ω_0 is the fundamental frequency. Our work goes beyond these studies and addresses (i) the fundamental understanding of $\chi_n(T,\omega_0)$, resulting from the overall magnetic hysteretic response near T_C in ultrathin ferromagnets, and (ii) more importantly, the independent determination of T_C. We therefore present, to our knowledge, for the first time measurements of $\chi_n(T)\equiv\chi_n(T,\omega_0)$ for ultrathin films up to $n=11$, and an analysis of *ac* susceptibility data in the vicinity of T_C. These higher-order contributions contain important information. We will show that with the knowledge of $\chi_n(T)$ one has the ability to extract temperature-dependent hysteresis loops close to T_C via a detailed Fourier analysis, and consequently the temperature dependence of the coercive field $H_C(T)$ and the saturation magnetization $M_S(T)$. This information is *not* accessible by measuring only the first component of the *ac* susceptibility $\chi(T)=\chi_1(T,\omega_0)$. T_C can be evaluated via two independent methods, namely, by the disappearance of $H_C(T)$ at T_C, and by the onset of the absorption signal $\chi_n''(T)$.[2]

To understand the origin of higher harmonic susceptibilities $\chi_n(T,\omega_0)$ we first discuss the response of a ferromagnetic system $\chi(T,H(t))$ due to a time-dependent external magnetic field $H(t)=H_0\cos(\omega_0 t)$ near T_C. It is well known[11] that $\chi(T,H(t))$ consists of both ferromagnetic and paramagnetic contributions. In the paramagnetic phase the order parameter $M(T,H(t))=|\mathbf{M}(T,H(t))|$ is proportional to the external magnetic field $H(t)$ as shown in Fig. 1(a), if the amplitude H_0 is small as compared to the thermal energy k_BT, where k_B is the Boltzmann constant. Hence, in this temperature regime $M(t)$ follows the oscillating magnetic field instantaneously without phase shift, as sketched in Fig. 1(b), resulting in a purely paramagnetic susceptibility.

In contrast, in the ferromagnetic phase, $M(T,H(t))$ is no longer in phase with $H(t)$, but hysteresis effects are ob-

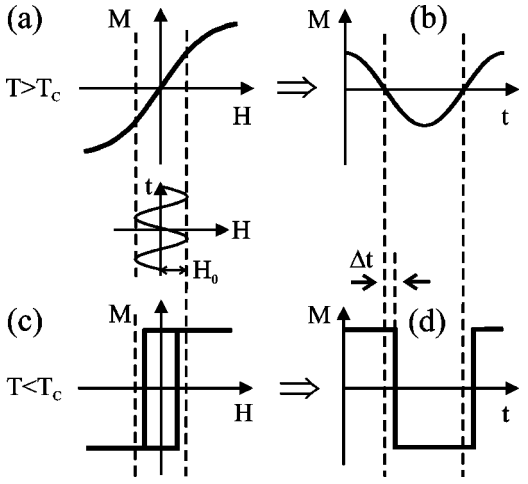

FIG. 1. Sketch of the field- and time-dependent magnetization $M(T,H(t))$ subject to an oscillating magnetic field $H(t)$ above and below T_C. (a) and (b) represent the paramagnetic case for $T>T_C$, whereas (c) and (d) show the magnetic response for $T<T_C$. The time shift Δt between $H(t)$ and $M(T,H(t))$ due to hysteretic effects is indicated (d). Note that the *y* axis *M* and the *x* axes *H* and *t* are not to scale. Small changes in $M(H)$ are therefore not visible.

served, see Fig. 1(c). To reverse the magnetization, as indicated by the vertical dashed lines, the modulation amplitude H_0 of the oscillating magnetic field has to be equal to or larger than the coercive field $H_C(T)$. In this case, $M(t)$ follows a discontinuous, almost square-shaped function exhibiting a time shift Δt with respect to $H(t)$, see Fig. 1(d). The temperature-dependent phase shift $\Delta\varphi(T)$ is given by $\Delta t = \Delta\varphi(T)\tau_0/(2\pi)$, with $\tau_0 = 2\pi/\omega_0$ the oscillation period. The corresponding response function $\chi(T,H(t))$ for $T<T_C$ can be described by a Fourier sum over the real and imaginary parts of the complex nth order susceptibility coefficients $\chi_n(T,\omega_0)=\chi_n'(T,\omega_0)+i\chi_n''(T,\omega_0)$:

$$\chi(T,H(t))=\sum_{n=-\infty}^{\infty}\chi_n(T,H_0,\omega_0)\exp(-in\omega_0 t). \qquad (2)$$

The Fourier components $\chi_n(T,\omega_0)$ can be directly determined through measurements of the *ac* susceptibility at multiples $n\omega_0$ of the fundamental frequency. Note that $\chi_n(T,H_0,\omega_0)$ is not field independent. As can be seen from Figs. 1(c) and 1(d), the phase shift $\Delta\varphi(T)$ can be expressed through $\sin\Delta\varphi(T)=H_C(T)/H_0$. For $T\to T_C^-$ and constant H_0 the area below the hysteresis curve as well as $\Delta\varphi(T)$ and $H_C(T)$ vanish. Obviously, for $T<T_C$ the magnetic response is a combination of both paramagnetic and ferromagnetic parts, $\chi_{pm}(T)$ and $\chi_{fm}(T)$. We will show in Sec. III, how these contributions can be separated in principle, and how the critical analysis can be improved. For a harmonic variation of $H(t)$ and if no bias fields are present, $M(T,H(t))$ exhibits an inversion symmetry, therefore only odd coefficients with $n=1,3,5,\ldots$ appear in Eq. (2).

The paper is structured as follows. After a short characterization of the experimental details in the following section we present and discuss the results of the measurements of $\chi_n(T,\omega_0)$ in Sec. III. In addition, we compare these results to calculations of higher harmonic susceptibilities in the vicinity of T_C in the framework of a *mean-field approximation* (MFA) which is described in detail in the Appendix. We conclude with a short outlook in Sec. IV.

II. EXPERIMENTAL DETAILS

The $(Fe_2/V_5)_{50}$ superlattices consist of two monolayers (ML) of Fe and 5 ML of V with a repetition rate of 50. This multilayer system was grown on a MgO(001) substrate through sputtering in an Ar atmosphere of 4×10^{-3} mbar at 630 K *in situ* in UHV. The structural and magnetic properties of our Fe/V samples are well known and have been investigated in detail by means of x-ray diffraction[12,13] and ferromagnetic resonance.[14] Lindner *et al.*[15] showed that $(Fe_2/V_5)_{50}$ exhibits a strong ferromagnetic interlayer exchange coupling $J'(T)$ through the V spacer layers, with $J_0'\approx100$ μeV/atom at $T\approx0$, corresponding to a large effective exchange field of ≈50 kOe. $J'(T)$ vanishes for $T\to T_C$ according to a power law $J'(T)\propto1-T^{3/2}$ in the ferromagnetic phase. Furthermore, the decoupling of the Fe layers for $T\to T_C^+$ could be independently confirmed through the absence of a dimensional crossover from two-dimensional to 3D behavior in these metallic superlattices.[2] In favor of this, *ac* susceptibility measurements on the same Fe/V sample were carried out in an extremely small oscillatory field with amplitude $H_0=17$ mOe. The critical analysis of the internal paramagnetic susceptibility $\chi_{pm}(T)=\chi_{1,pm}'(T)$ according to Eq. (1) yields a 2D Ising-like critical exponent $\gamma=1.72(18)$ above the Curie temperature $T_C=304.75(15)$ K. This value of T_C was determined independently by the onset of the absorption signal $\chi_1''(T)$ and is used in the following considerations.

Both real and imaginary parts $\chi_n'(T)$ and $\chi_n''(T)$ of the complex quasistatic susceptibility are measured using a classical mutual inductance (MI) bridge calibrated in SI units.[16] In our particular setup, $\chi_n(T)$ is directly proportional to the difference between the induction signals of two identical secondary coils, measured with and without the sample. The MI setup is characterized by a high sensitivity of ≈1 ML of Ni at $H_0=275$ mOe providing a minimum signal-to-noise ratio of 2:1. Oscillating magnetic fields $H(t)=H_0\cos(\omega_0 t)$ with amplitudes H_0 between 17 mOe and 1.6 Oe are accessible. After subtraction of a linear background all susceptibility spectra were normalized to the field amplitude H_0, the frequency, and the volume of the ferromagnetic layers. Our unique MI setup is calibrated with a paramagnetic substance of well-known susceptibility. Therefore, the $\chi_n(T)$ are given in absolute SI units which is not easily possible using alternative magnetometries, e.g., the magneto-optical Kerr-effect.

For the measurements of the Fe/V superlattices reported here, $\chi_n'(T)$ and $\chi_n''(T)$ were simultaneously recorded at particular frequencies $n\omega_0$ at fixed excitation frequency $\nu_0=\omega_0/(2\pi)=213$ Hz and amplitude $H_0=0.8$ Oe using lock-in technique. $H(t)$ was applied along the easy axis of magnetization which is the in-plane Fe[110] direction.[2] The use of very small field amplitudes, low oscillation frequencies, as well as extremely small temperature rates (3–5 mK/s) is mandatory for an accurate determination of the proper initial zero-field susceptibility. Remaining static laboratory fields, e.g., the earth-magnetic field, have to be compensated with sufficient accuracy, which in our setup is better than 10 mOe using a pair of calibrated Helmholtz coils. An alternative and indirect, but rather accurate, proof for best compensation of such static fields is provided by the measurement of the second harmonic coefficient $\chi_2(T)$ which should vanish for a purely sinusoidal field $H(t)$. This requirement is fulfilled for all data sets presented here over the whole range of amplitudes of the oscillatory magnetic field up to 1.6 Oe. The measurements of the odd harmonics were performed in a temperature range between 280 K and 360 K, corresponding to reduced temperatures $0.92<T/T_C<1.2$. The relative accuracy of the temperature determination is obtained to be ±50 mK. The error bar for the absolute temperature is significantly larger, however is of no relevance in the present case.

We would like to give some general remarks concerning *ac* and *dc* measurements. Considering the *ac* susceptibility, it is important to note that if the amplitude H_0 of the oscillating magnetic field is smaller than $H_C(T)$, a ferromagnetic contribution $\chi_{fm}(T)$ results from a partial reversal of magnetic domains. On the other hand, if H_0 is larger than $H_C(T)$, a

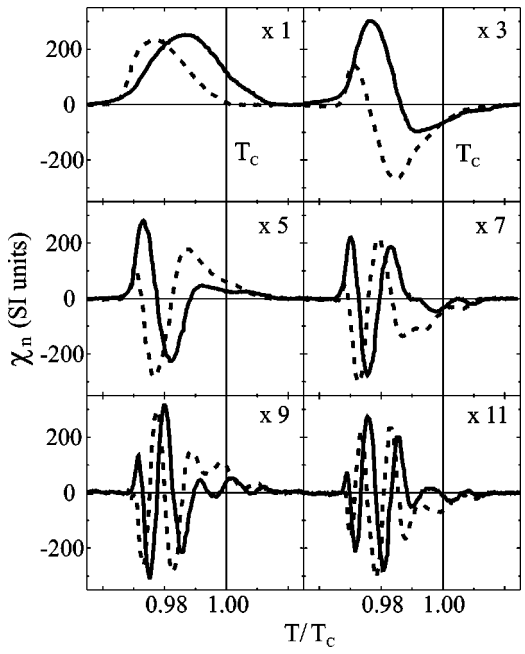

FIG. 2. Measured real parts $\chi_n'(T)$ (solid lines) and imaginary parts $\chi_n''(T)$ (dashed lines) of the *ac* susceptibility for the $(Fe_2/V_5)_{50}$ superlattice. These quantities are scaled by the order n as indicated by the magnification factors ($\times n$). The Curie temperature $T_C = 304.75(15)$ K is represented by the vertical solid lines.

complete magnetic reversal will occur via domain-wall motion. Although in this case $\chi_{fm}(T)$ is correlated to the temperature-dependent magnetic anisotropy $K(T)$ of the thin-film system, as given, e.g., by the phenomenological model of Callen and Callen,[17] this magnetic reversal is far from being well understood since it is strongly dominated by the structural perfection of the investigated sample. Although measurements of the *dc* susceptibility[18] do not deal with effects resulting from oscillating magnetic fields, there are a number of disadvantages, namely, (i) the measurement of the vanishing order parameter $M(T)$ which usually demands the application of larger magnetic fields H_0 and this in turn blurs the phase transition, (ii) the lack of an absorption signal that allows for an independent determination of T_C, and (iii) the usually smaller temperature resolution as compared to *ac* measurements due to technical reasons especially for thin films.

III. RESULTS AND DISCUSSION

A. Higher harmonic susceptibilities

In order to fully understand the entire magnetic response on an oscillatory magnetic field $H(t)$ in the vicinity of T_C, we have performed temperature-dependent measurements of a number of higher harmonic susceptibilities $\chi_n(T) = \chi_n'(T) + i\chi_n''(T)$ up to $n = 11$. Figure 2 shows the real and imaginary Fourier components $\chi_n'(T)$ and $\chi_n''(T)$ determined for Fe_2/V_5. In order to obtain a similar scaling of the y axis, $\chi_n'(T)$ and $\chi_n''(T)$ have been multiplied by the factor n.

Due to the high sensitivity of our MI setup and the large number of Fe layers in the Fe/V sample it was possible to obtain nearly noise-free susceptibility spectra with a signal-to-noise ratio of better than 50:1. We emphasize that T_C is not located at the maximum of $\chi_1'(T)$, but at the temperature where $\chi_1''(T)$ vanishes.[2] Moreover, the maximum of $\chi_1'(T)$ results from the ferromagnetic contribution $\chi_{1,fm}(T)$ originating from magnetic reversals and/or domain walls driven by the oscillating field $H(t)$. The first harmonic $\chi_1(T)$ is a positive quantity, with a maximum of 250 SI units and a full-width half-maximum (FWHM) of 6.5 K. The higher harmonic susceptibilities $\chi_3(T)$, $\chi_5(T)$, etc. consist of both positive and negative parts. Decreasing the modulation amplitude below $H_0 = 70$ mOe decreases the width of the susceptibility peak to 3 K, which is the stable minimum FWHM. In addition, a strong dependence between the order n and the peak shape of the higher harmonic susceptibilities might exist due to the fact that the signals narrow with increasing n. Furthermore, the number of oscillations of $\chi_n(T)$ is directly correlated to n. Each harmonic susceptibility exhibits $(n+3)/2$ zeros and $(n+1)/2$ extrema. In addition, the amplitudes of $\chi_n(T)$ scale with $1/n$, as is visible in Fig. 2. To our knowledge these are the first experimental results presenting such a large variety of noise-free higher-order harmonics of the *ac* susceptibility for ultrathin ferromagnets.

The Fourier coefficients of the magnetization $M_n(T) = H_0\chi_n(T)$ are calculated in the Appendix with the help of a Heisenberg Hamiltonian. Analytical expressions for these coefficients, as well as for their zeros, can be deduced close to the Curie temperature by application of MFA and additional approximations. For the real and imaginary parts of the higher harmonics we obtain

$$M'_{n,fm}(T) = \frac{2M_0(T)}{n\pi}\sin(n\omega_0\tau^*), \tag{3}$$

$$M''_{n,fm}(T) = -\frac{2M_0(T)}{n\pi}\cos(n\omega_0\tau^*). \tag{4}$$

A quartic anisotropy is assumed, corresponding to the Fe/V(001) system under consideration. The anisotropy parameter K_4 is chosen in order to reproduce the strong increase of the response signal at $T_0/T_C \simeq 0.97$, see Fig. 2, yielding $K_4 = 0.0588$ K/atom $= 5$ μeV/atom $= 7 \cdot 10^5$ erg/cm^3. Moreover, a magnetic moment of $\mu_{Fe} = 2.25$ μ_B is assumed. Figure 3 shows the real and imaginary parts of the susceptibility coefficients $\chi_n(T)$ for a field amplitude $H_0 = 0.8$ Oe. The magnitudes of $\chi_n'(T)$ and $\chi_n''(T)$ are scaled by a common factor in order that the maximum of $\chi_1'(T)$ coincides with the measured one. Furthermore, these quantities are multiplied by the factor n, in correspondence with Fig. 2.

Obviously, although this simple mean-field approach does not allow for a quantitative comparison to experiment, it reproduces quite well the main experimental findings. The overall oscillating behavior, the relative order of the extrema, and the number of zeros of $\chi_n(T)$ coincide, as does the $1/n$ dependence of the amplitudes. Large values for both $\chi_n'(T)$ and $\chi_n''(T)$ are obtained in the temperature range $T_0 < T < T_C$ where magnetic reversals over energy barriers are effective. Evidently, this ferromagnetic response due to mag-

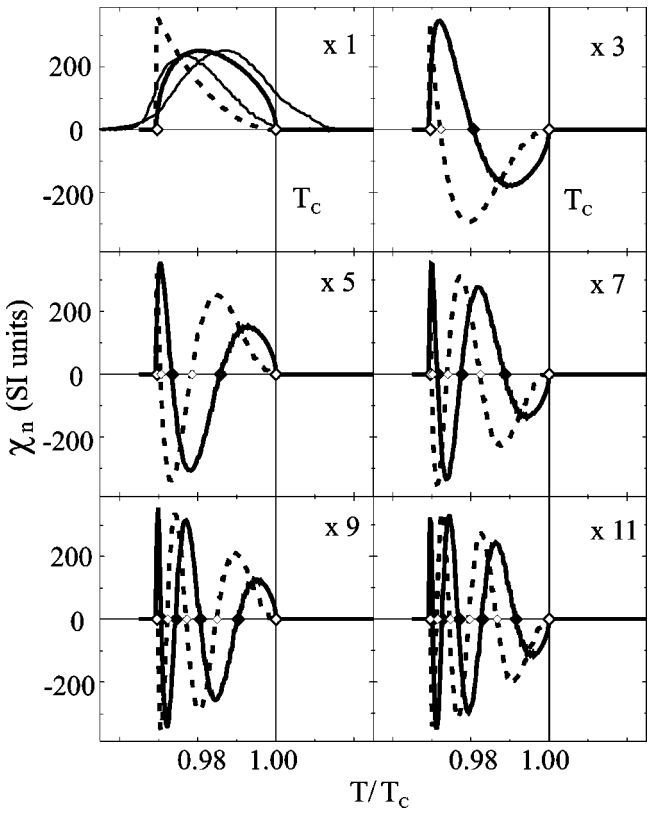

FIG. 3. Real parts $\chi_n'(T)$ (thick solid lines) and imaginary parts $\chi_n''(T)$ (dashed lines) calculated numerically via MFA. The spectra are scaled by a common factor in order that the maximum of $\chi_1'(T)$ coincides with the measured one, see Fig. 2. Moreover, $\chi_n'(T)$ and $\chi_n''(T)$ are multiplied by *n*. The zeros of $\chi_n'(T)$ and $\chi_n''(T)$ as given by Eq. (A18) are indicated by the filled and open symbols, respectively. For comparison, the measured $\chi_1'(T)$ and $\chi_1''(T)$ are also plotted (thin lines).

netic rotation yields a much larger signal as compared to the paramagnetic one resulting from variation of the magnitude of the magnetization. The latter response is present for all temperatures, yielding small but finite real parts $\chi_n'(T)$ and vanishing absorption parts $\chi_n''(T)$. Since the field amplitude is very small this contribution can hardly be observed on the scale as presented in Fig. 3. Furthermore, for $T \lesssim T_C$ the zeros of the ferromagnetic coefficients are analytically given by Eq. (A18). However, for temperatures very close to T_C the approximation of Eq. (A8) breaks down since it yields a divergence of $\chi_{1,pm}'(T)$ at T_C, see Eq. (A11), which is not present for the numerically obtained results as presented in Fig. 3. Also, finite values for $\chi_{n,pm}'(T)$ with $n>1$ are present which are not reproduced by this approximation. We note in passing that the only fitting parameter applied in the calculations is the value of K_4, whereas the other quantities are provided independently.

We like to point out several shortcomings of the theoretical results. The MFA is known to yield at least qualitatively correct results also for anisotropic 2D ferromagnets.[19] Since collective magnetic excitations are not taken into account, the induced magnetization for $T \gtrsim T_C$ is very small, which is in fact an order of magnitude larger due to the alignment of *spin blocks* rather than single spins as in the present calculations.[20] Moreover, as mentioned in the Appendix, the theory is not able to reproduce the left shoulders of $\chi_n(T)$ below $T_0/T_C=0.97$, see Fig. 3. Although in this temperature range the field amplitude H_0 is smaller than the coercive field H_C, large $\chi_n'(T)$ and finite absorption signals $\chi_n''(T)$ are most probably caused by the formation and partial reversal of magnetic domains which is not included in the theory. The calculation yields sharp kinks of $\chi_n'(T)$ and $\chi_n''(T)$ at $T_0/T_C \simeq 0.97$, which are not present in the experimental data. Moreover, the intensities of the measured low-temperature maxima of $\chi_n(T)$ are systematically damped with respect to the calculated ones, especially for the higher harmonics. In particular, the first maxima of $\chi_n''(T)$ at $T_0/T_C=0.97$ decrease with increasing *n* and finally disappear for $n=9$ and $n=11$, whereas theory predicts always a positive value for $\chi_n''(T_0)$ at the onset of the magnetic reversal. This discrepancy between theory and experiment could be caused by an intrinsic structural inhomogeneity of the Fe/V superlattice, resulting in layer-dependent strengths of the anisotropy and in different directions of the corresponding easy axes. Therefore, the magnetic reversals of the individual Fe layers happen at slightly different magnetic fields. Also, thermal assisted crossing of energy barriers may be present in this temperature range which is also not accounted for theoretically. These processes will reduce the maxima of $\chi_n'(T)$ near T_0/T_C. In addition, a finite absorption may occur below T_0.

B. Coercive field close to T_C

In this section we determine the hysteresis loops, the coercive field $H_C(T)$, and the saturation magnetization $M_S(T)$ out of the measurements of $\chi_n(T)$ in the vicinity of the Curie temperature T_C with a large accuracy. As mentioned above, the relative temperature resolution of our MI setup is ≈ 50 mK. Hence, the $\chi_n(T)$ data were taken in relative temperature intervals of about $\Delta T/T_C \approx 1.6\times 10^{-4}$, yielding nearly 200 hysteresis loops in a small temperature range of $\approx 4\%$ around T_C. Furthermore, it is possible to increase the accuracy by a factor of 5–10 through linear interpolation of $\chi_n(T)$. By performing a numerical Fourier analysis from the measured data the magnetizations $M(t)$ and $M(H)$ as functions of time *t* and magnetic field *H* are shown in Figs. 4 and 5 for different relative temperatures ranging between $T/T_C=0.975$ and 1.01. The presented time range corresponds to a single oscillation period $\tau_0=1/\nu_0$, with $\nu_0=213$ Hz, i.e., a single hysteresis loop. Note that only Fourier coefficients up to order $n=11$ are considered, resulting at first glance in a very ragged magnetization behavior. Nevertheless, the main features of the $M(t)$ and $M(H)$ curves can be easily extracted. For $T/T_C<1$ the magnetizations follow an almost square-shaped overall behavior, with a phase shift $\sin\Delta\varphi(T)=H_C(T)/H_0$ between $H(t)$ and $M(t)$ which decreases with increasing T/T_C. Below $T_0/T_C=0.97$ only minor loops result due to the limited modulation amplitude H_0. On the other hand, in the paramagnetic phase $M(t)$ follows $H(t)$ instantaneously with $\Delta\varphi(T)=0$, and exhibits an almost sinusoidal overall behavior.

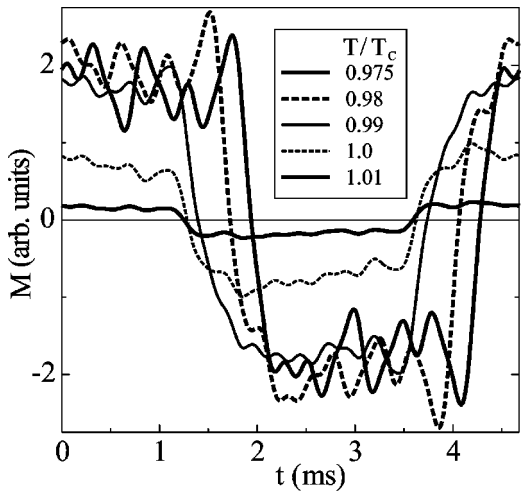

FIG. 4. Time-dependent magnetizations $M(t)$ calculated via a Fourier analysis of the measured susceptibility coefficients $\chi_n(T)$, see Fig. 2, for reduced temperatures $0.975<T/T_C<1.01$ as indicated. Fourier coefficients up to order $n=11$ have been used. For the sake of clarity only an assortment of square functions is shown.

The oscillations of $M(t)$ and $M(H)$ observed in Figs. 4 and 5 result mainly from the fact that only a comparably small number of Fourier coefficients have been used for the analysis. This so-called *Fourier ringing* will be present also if much more susceptibility coefficients will be considered. In particular, the oscillations will become more pronounced if the magnetization curves become increasingly rectangular. Nevertheless, we emphasize that the overall quantities such as $H_C(T)$ and $M_S(T)$ can be determined with high accuracy also from a limited number of Fourier coefficients.

In Fig. 6 the saturation magnetization $M_S(T)$ and the coercive field $H_C(T)$, which have been extracted from Figs. 4 and 5, are presented as a function of the reduced temperature T/T_C. As a matter of fact, these quantities exhibit the same large temperature resolution of about 10^{-4} like the susceptibilities, and an excellent signal-to-noise ratio which cannot be achieved in the vicinity of T_C using conventional direct magnetization measurements. For comparison, also the corresponding quantities calculated by MFA are given. $M_S(T)$

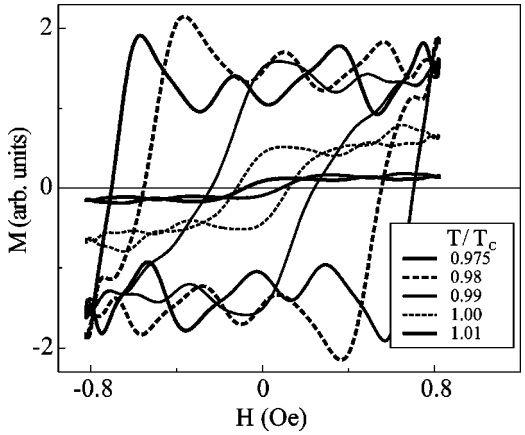

FIG. 5. Hysteresis loops $M(H)$ for different reduced temperatures T/T_C corresponding to Fig. 4.

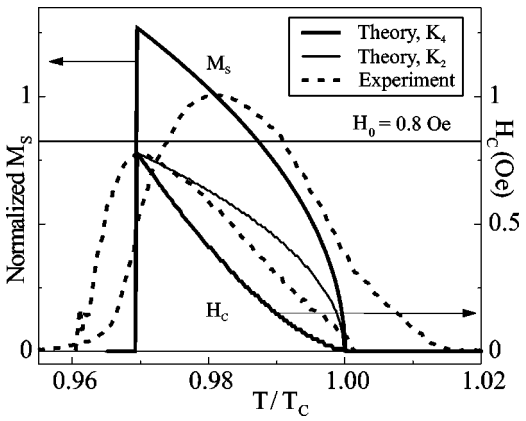

FIG. 6. Comparison of theoretically and experimentally determined saturation magnetization $M_S(T)$, normalized to unity (left axis), and the coercive field $H_C(T)$ in units of Oe (right axis) as a function of the reduced temperature T/T_C. $H_C(T)$ has been calculated for both a uniaxial (K_2) and a quartic (K_4) in-plane anisotropy.

shows a broad maximum at $T/T_C\approx 0.98$ located between the maxima of $\chi_1'(T)$ and $\chi_1''(T)$. Obviously, below this temperature H_0 is not large enough to saturate the Fe/V sample. Moreover, $M_S(T)$ exhibits a significant nonzero contribution above T_C up to $T/T_C\approx 1.015$ induced by the oscillating magnetic field. Theoretically, $M_S(T)$ is defined as $M_S=[M(t=0)-M(t=\tau_0/2)]/2=[M(H=H_0)-M(H=-H_0)]/2$, which almost vanishes for $T<T_0=0.97\ T_C$. The very small induced magnetization above T_C is not visible in Fig. 6.

The coercive field $H_C(T)$ as determined from measurements exhibits a maximum at $T/T_C=0.97$. Evidently, for $T/T_C>0.97$ the amplitude $H_0=0.8$ Oe of the oscillating magnetic field is larger than $H_C(T)$. In this temperature range $H_C(T)$ decreases almost linearly, and vanishes for $T\rightarrow T_C$. Very close to T_C a curvature is observed. Below $T_0/T_C=0.97$ a finite $H_C(T)$ is obtained which is most probably caused by partial reversals of magnetic domains.

From the theoretical point of view we like to point out a qualitatively different behavior of $H_C(T)$ obtained from the uniaxial and quartic in-plane anisotropy. Here, the parameter K_2 is assumed in order to obtain $T_0/T_C=0.97$, resulting in $K_2=4.43\times 10^{-4}$ K/atom, which is two orders of magnitude smaller than the applied value for K_4. $H_C(T)$ as obtained from the uniaxial anisotropy exhibits an *upward* curvature. In contrast, $H_C(T)$ calculated from the quartic anisotropy shows a *linear* behavior over a wide range of reduced temperatures, and approaches T_C with a *downward* curvature. As can be seen from Fig. 6, the calculated $H_C(T)$ for a quartic anisotropy compares much better to the measurement, which is evident from the underlying in-plane symmetry of the Fe/V(001) superlattice.

C. Paramagnetic and ferromagnetic contributions

We show in the following that the *ac* susceptibility can be separated into the paramagnetic and ferromagnetic contributions $\chi_{fm}(T)$ and $\chi_{pm}(T)$ both in theory and, in principle, experimentally.

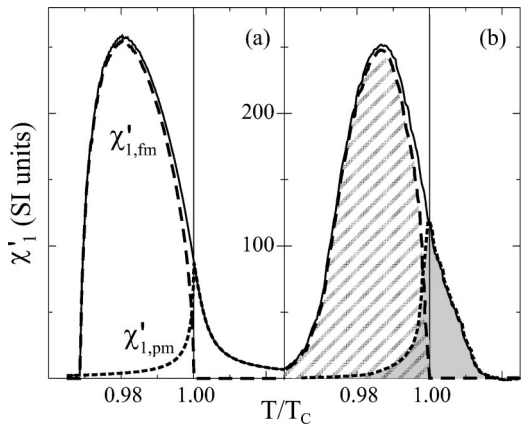

FIG. 7. Separation of the first harmonic coefficient $\chi_1'(T) = \chi_{1,fm}'(T) + \chi_{1,pm}'(T)$ into a ferromagnetic (long dashed) and a paramagnetic part (short dashed). (a) Theory and (b) Experiment. In (b) the paramagnetic and ferromagnetic contributions (hatched areas) are drawn by a simplified procedure, see text.

Theoretically, $\chi_{pm}(T)$ is determined from the calculations by not allowing for the magnetization jump $M(T) \rightarrow -M(T)$, $\chi_{fm}(T)$ being then simply the difference between $\chi(T)$ and $\chi_{pm}(T)$. This analysis can be performed independently for all orders n of the Fourier coefficients $\chi_n(T)$. In Fig. 7(a) the results for $\chi_1'(T)$ are depicted. In order to obtain a sizeable paramagnetic contribution, we have applied a large modulation amplitude $H_0 = 800$ Oe. Clearly, as $\chi_{1,fm}'(T)$ vanishes for $T \rightarrow T_C$, $\chi_{1,pm}'(T)$ exhibits a maximum at T_C as expected from general considerations. Since the latter contribution is small, this maximum does not appear in the full susceptibility $\chi_1'(T)$. For other parameters an additional (small) maximum of $\chi_1'(T)$ may show up at T_C. Making use of the approximation of Eq. (A8), the ferromagnetic and paramagnetic parts of $\chi(T)$ are given analytically by Eqs. (3), (4), and (A11). This approximation yields a paramagnetic contribution for only the $(n=1)$ coefficient, which diverges at T_C.

Experimentally, the separation of $\chi(T)$ into a ferromagnetic and a paramagnetic part can be performed through the measurements of $\chi_n(T)$ as presented in Fig. 2. Therefore, the corresponding hysteresis loops, see Fig. 5, are approximated by ideal rectangular loops. The subsequent Fourier analysis yields the ferromagnetic susceptibility coefficients $\chi_{n,fm}(T)$. The paramagnetic parts $\chi_{n,pm}(T)$ can be obtained from the loops of Fig. 5 either through the linear background or by subtracting the ferromagnetic contribution. Since we have not finished our analysis yet, we do not present the separation into $\chi_{n,fm}(T)$ and $\chi_{n,pm}(T)$ from experimental data explicitly. Merely, a simplified procedure can be done by subtracting the *calculated* $\chi_{n,pm}'(T)$, see Fig. 7(a), from the *measured* $\chi_n'(T)$ for $T < T_C$, assuming $\chi_{n,pm}'(T) = \chi_n'(T)$ for $T \geqslant T_C$. The result for $n=1$ is shown in Fig. 7(b). Both contributions are characterized by the hatched areas.

Although the study of critical phenomena in the vicinity of T_c is not the focal point of our work, we discuss a future application of measured higher harmonic susceptibility data. The analysis of critical phenomena can in principle be improved considerably by taking advantage of two properties. First, an accurate fit of $\chi_{pm}(T)$ according to Eq. (1) needs the separate knowledge of T_C. In our analysis T_C is determined independently by the temperature where $H_C(T)$ disappears. Moreover, it is proven that T_C is not located at the maximum of $\chi_1'(T)$. It is important to note that the maximum (or singularity) of $\chi_1'(T)$ is located exactly at the Curie temperature T_C only for infinitesimal small fields. Furthermore, the definition of T_C as the temperature where the absorption signal $\chi_1''(T)$ disappears[2] is confirmed. Second, the separation of $\chi_n(T)$ into $\chi_{n,fm}(T)$ and $\chi_{n,pm}(T)$ close to T_C yields the possibility to determine the critical exponent γ, Eq. (1), on *both* sides of the phase transition. Note that this is possible for every higher harmonic $\chi_{n,pm}'(T)$.

IV. CONCLUSION AND OUTLOOK

We have performed temperature-dependent measurements of the higher harmonic susceptibilities $\chi_n(T)$ up to $n=11$ for ferromagnetic Fe_2/V_5 superlattices. A detailed Fourier analysis of the *ac* susceptibility data yields hysteresis loops in the vicinity of the Curie temperature T_C as a function of temperature. The coercive field $H_C(T)$ as well as the saturation magnetization $M_S(T)$ are accessible in a very small temperature range of $\approx 4\%$ around T_C with a large temperature resolution of $\Delta T/T_C = 2 \times 10^{-4}$ and a signal-to-noise ratio which is hardly accessible using direct magnetization measurements. We have shown the following.

(i) The detection and analysis of $\chi_n(T)$ allow for an independent determination of T_C via the temperature dependence of $H_C(T)$. Obviously, T_C is not located at the maximum of $\chi_1'(T)$, which confirms our previous determination of T_C via the onset of $\chi_1''(T)$.[2]

(ii) This analysis in principle gives the possibility to separate the para- and ferromagnetic parts of the susceptibility with experimental means.

For comparison, we have calculated $\chi_n(T)$ within a mean-field approach, as well as $H_C(T)$ and $M_S(T)$. The simplicity of this method allows for an analytical representation of the Fourier coefficients $\chi_n'(T)$ and $\chi_n''(T)$, and of their zeros close to T_C. A satisfactory agreement between theory and experiment is obtained. A different behavior of $H_C(T)$ results by considering a uniaxial and a quartic in-plane anisotropy.

The use of the MFA is expected to give qualitative correct results of the magnetic properties also for anisotropic 2D systems. For a quantitative comparison one has to apply improved methods, e.g., a Green's function theory.[19,21] In particular, for layered systems the consideration of collective magnetic excitations (spin waves) is very important. As a drawback, analytical expressions for, e.g., the magnetization coefficients $M_n(T)$ are not easily accessible within these improved theories. In correspondence with the Fe/V(001) system, we have considered a quartic anisotropy whose easy axis coincides with the direction of the external magnetic field. The consideration of an angle between easy axis and field direction is also feasible. If a constant bias field is applied or if the oscillating field contains higher harmonics,

even Fourier coefficients for the magnetization will appear.

Future experimental work has to improve the interplay between the use of smaller modulation amplitudes $H_0 < 0.8$ Oe and the sensitivity of the MI setup, in order to yield a larger number of higher harmonic susceptibilities with $n > 11$. Furthermore, the separation of the *ac* susceptibility into ferromagnetic and paramagnetic parts out of the experimental data has to be performed. These facts, including the use of even smaller H_0, provide the possibility to determine the critical behavior from susceptibility data on more safe ground as compared to previous work. In particular, an accurate determination of the proper critical exponent γ of the paramagnetic susceptibility seems to be possible by analyzing the higher harmonic response $\chi_n(T)$ within a single experiment with high accuracy.

ACKNOWLEDGMENTS

This work was supported by the Deutsche Forschungsgemeinschaft, SFB 290, TP's A1 and A2, and the Swedish Foundation of Strategic Research (SSF). P. Blomquist and R. Wäppling are thanked for preparing the samples.

APPENDIX: THEORETICAL MODEL

The Fourier coefficients $M_n(T,\omega_0)$ of the magnetization $M(T,H)$, which is time dependent through the oscillating magnetic field $H(t)$, are given by

$$M_n(T,\omega_0) = \frac{1}{\tau_0}\int_0^{\tau_0} dt M(T,H)\exp(in\omega_0 t), \qquad \text{(A1)}$$

yielding the real (in-phase) and imaginary (out-of-phase) coefficients $M_n(T) = M_n'(T) + iM_n''(T)$ to order n. For this purpose a Heisenberg-type Hamilton is applied, considering for simplicity classical spins[22] with unit length $|\mathbf{S}_i| = 1$ on lattice sites i:

$$\mathcal{H} = -\frac{J}{2}\sum_{\langle i,j\rangle} \mathbf{S}_i\mathbf{S}_j - K_2\sum_i (S_i^z)^2 - K_4\sum_i (S_i^x)^2(S_i^z)^2 - \mu_0\mu\sum_i H(t)S_i^z. \qquad \text{(A2)}$$

$J>0$ is the ferromagnetic exchange coupling between nearest-neighbor spins i and j. For the sake of comparison both uniaxial and quartic in-plane anisotropies are considered, whose strengths are denoted by K_2 and K_4. Positive values of these quantities indicate an easy axes directed along the cardinal (x or z) axes of the square lattice. The proper symmetry of this in-plane anisotropy should correspond to the underlying lattice symmetry,[23] which is the quartic one for the $Fe_2/V_5(001)$ superlattice. K_2 or K_4 are used as fit parameters in order to reproduce the measured coercive field H_C. The oscillating external magnetic field $H(t) = H_0\cos(\omega_0 t)$ with amplitude H_0 and frequency ω_0 is directed along the z axis, μ is the atomic magnetic moment, and μ_0 the vacuum permeability.

The Hamiltonian, Eq. (A2), is solved by a MFA, assuming a ferromagnetic order characterized by the magnetization $M(T,H) = \mu\langle S_i^z\rangle$. Depending on the relative strength of magnetic field and anisotropy one has to distinguish two cases. First, the $+z$- and $-z$ directions, referring to the in-plane angles $\phi = 0$ and $\phi = \pi$, represent a minimum and a maximum of the free energy $F(T,H,\phi)$. Second, these two directions are both minima of $F(T,H,\phi)$, separated by an energy barrier. If the magnetic field is too weak to overcome this energy barrier, the effect of $H(t)$ results in a small variation of the magnetization around the remanent magnetization $M(T,0) = M_0(T)$. In this case no magnetic hysteresis will occur, nor an energy dissipation. On the other hand, if at some instant of time the oscillating field $H(t)$ is strong enough to surpass the anisotropy barrier, a magnetic reversal takes place and magnetic hysteresis accompanied by energy uptake occurs. It is important to notice that thermal assisted crossing of energy barriers is not considered within this study. Also, since a uniform system is assumed, magnetic reversals mediated by domain-wall movements cannot be taken into account. Moreover, thermal fluctuations above the Curie temperature T_C, which may result in energy dissipation, are neglected by the MFA.

In general, the determination of the free energy $F(T,H,\phi)$, as well as the magnetizations $M(T,H)$ and $M_n(T,\omega_0)$, is performed numerically, see Fig. 3. Analytical expressions for these quantities are derived as described in the following sections.

1. Small anisotropies

Since for $3d$ transition-metal magnets the exchange interaction is much stronger than the anisotropy, i.e., $J \gg K_2, K_4$, the latter is handled as a small perturbation. In this case the magnitude of the magnetization is given by the Langevin function $M(T,H(t)) = \mu[\coth(x) - 1/x]$, with $x = [qJM(T,H(t)) + \mu_0\mu H(t)]/(k_BT)$ and q the coordination number. Within this approximation the Curie temperature is given by $k_BT_C = qJ/3$.

The anisotropies are considered by a thermodynamic perturbation theory,[24] yielding the *effective, temperature-dependent anisotropy coefficients* $\mathcal{K}_2(T,H) = K_2 f_2(T,H)$ and $\mathcal{K}_4(T,H) = K_4 f_4(T,H)$. The functions $f_2(T,H)$ and $f_4(T,H)$ depend on temperature mainly through the magnetization and read

$$f_2(T,H) = 1 - \frac{3}{x}\coth(x) + \frac{3}{x^2}, \qquad \text{(A3)}$$

$$f_4(T,H) = 1 - \left(\frac{10}{x} + \frac{105}{x^3}\right)\coth(x) + \frac{45}{x^2} + \frac{105}{x^4}. \qquad \text{(A4)}$$

Note that $\mathcal{K}_{2,4}(T,H) \to K_{2,4}$ for $T \to 0$, and $\mathcal{K}_{2,4}(T,0) \to 0$ for $T \to T_C$. The decreasing effective anisotropies $\mathcal{K}_2(T,H)$ and $\mathcal{K}_4(T,H)$ account for the fact that with increasing temperature the ability of the anisotropies to maintain a particular direction of the magnetization decreases. Moreover, to a good approximation the *angle dependent* part of the free energy is given by[24]

$$F(T,H,\phi) = -\mu_0\mu H(t)M(T,H)\cos\phi - K_2 f_2(T,H)\cos^2\phi - K_4 f_4(T,H)(\cos^4\phi - \cos^2\phi). \quad \text{(A5)}$$

Here a weak dependence of $M(T,H)$ on ϕ is neglected. Minimization of $F(T,H,\phi)$ with respect to ϕ yields the (meta)stable directions of the magnetization. The condition that both directions $\phi=0$ and $\phi=\pi$ refer to minima requires that $\mu_0\mu H(t)M(T,H) + 2[K_2 f_2(T) + K_4 f_4(T)] > 0$. The time instant τ^* within an oscillation period $\tau_0 = 2\pi/\omega_0$, at which a magnetic reversal happens, depends on temperature and is given by

$$\cos(\omega_0\tau^*) = -\frac{2[K_2 f_2(T,H(\tau^*)) + K_4 f_4(T,H(\tau^*))]}{\mu_0\mu H_0 M(T,H(\tau^*))}. \quad \text{(A6)}$$

For a harmonic oscillation and if no bias field is present, the backward magnetic reversal happens at time $\tau^* + \tau_0/2$. The effect of the magnetic field can be separated into (i) a variation of the magnitude (length) of the magnetization $M(T,H)$ and (ii) a magnetic reversal (jump) with constant length. Whereas the former is present for all temperatures, the latter is nonvanishing only in those temperature ranges $T_0 < T < T_C$ where an anisotropy barrier is present and which can be surmounted during the field oscillation, resulting in a magnetic hysteresis. Only in the presence of a magnetic hysteresis an absorptive part $\chi''(T) > 0$ of the susceptibility exists, if no other processes such as partial domain reversals or thermal assisted crossings of energy barriers are considered. The temperature T_0 is implicitly given by

$$\mu_0\mu H_0 M(T_0,-H_0) = 2[K_2 f_2(T_0,-H_0) + K_4 f_4(T_0,-H_0)]. \quad \text{(A7)}$$

In the following section the two contributions (i) and (ii) are studied separately.

2. Small magnetic fields

For small Zeeman energies (small field amplitudes H_0) as compared to the thermal energy $k_B T$ near T_C the Langevin function is expanded to first order in $H(t)$:

$$M(T,H) \simeq M(T,0) + \Delta M(T,H) = M_0(T) + \chi(T,0)H(t). \quad \text{(A8)}$$

Here $M_0(T)$ denotes either the positive $[M_0(T) > 0]$ or the negative value $[M_0(T) < 0]$ of the remanent magnetization during the hysteresis loop as sketched in Fig. 1(c). The susceptibility $\chi(T,H) = \partial M(T,H)/\partial H$ within MFA is calculated for classical spins to be

$$\frac{\mu_0\mu^2}{\chi(T,H)} = \frac{k_B T x^2 \sinh^2(x)}{\sinh^2(x) - x^2} - 3k_B T_C, \quad \text{(A9)}$$

where x is given in the text above Eq. (A3). For $T > T_C$ and $H_0 = 0$ the limiting behavior $\chi(T,0) = (\mu_0\mu^2)/[3k_B(T - T_C)]$ results. Note that the approximation Eq. (A8) is not valid for temperatures very close to T_C. Here a nonlinear behavior of $M(T,H)$ with respect to H is present, given by $M(T_C,H) \simeq H^{1/\delta}$, with the critical exponent $\delta = 3$ within MFA.[1] Calculations show that this nonlinear behavior dominates for $0.995 < T/T_C < 1.005$.

First we consider the rectangular part of $M(T,H)$ in the temperature range $T_0 < T < T_C$. As function of t the magnetization jumps between $M_0(T) \leftrightarrow -M_0(T)$ at time instants τ^* and $\tau^* + \tau_0/2$ during an oscillation period. This rectangular function is shifted by Δt with respect to the *ac* field, see Fig. 1(d). As can be seen from Eq. (A6), within the employed approximations τ^* is given by

$$\cos(\omega_0\tau^*) \simeq -\frac{2[K_2 f_2(T,0) + K_4 f_4(T,0)]}{\mu_0\mu H_0 M_0(T)}. \quad \text{(A10)}$$

The Fourier transformation of the rectangular function yields the real and imaginary parts $M'_{n,fm}(T)$ and $M''_{n,fm}(T)$ given by Eqs. (3) and (4) in the main text. We call these parts the *ferromagnetic contribution*, since they result exclusively from a reversal of the magnetization. Only odd coefficients appear $(n = 1,3,5,\ldots)$, the even coefficients $(n = 0,2,4,\ldots)$ vanish due to inversion symmetry of $H(t)$. The amplitudes of the Fourier coefficients vary with increasing order as $1/n$. Both real and imaginary Fourier coefficients $M'_{n,fm}(T)$ and $M''_{n,fm}(T)$ vanish for $T \to T_C$, since $M_0(T) \to 0$. Finally, one observes that the zeros of the Fourier coefficients $M'_{n,fm}(T)$ coincide with the extrema of $M''_{n,fm}(T)$, and vice versa. These zeros will be discussed in the following section.

The Fourier transformation of $\Delta M(T,H)$, see Eq. (A8), yields a contribution $M'_{1,pm}(T)$ only to the real part of the $n=1$–coefficient. This is a *paramagnetic contribution* since it originates exclusively from the variation of the length of $M(T,H)$. $M'_{1,pm}(T)$ does not depend on ω_0 and is present for all temperatures:

$$M'_{1,pm}(T) = \tfrac{1}{2}\chi(T,0)H_0. \quad \text{(A11)}$$

Note that $M'_{1,pm}(T)$ exhibits a singularity at $T = T_C$ which is an artifact of the approximation, Eq. (A8). The total real $n = 1$–Fourier coefficient is the sum of Eqs. (3) and (A11).

3. Zeros of the Fourier coefficients

In this section we derive analytical expressions for the zeros of the Fourier coefficients $M'_{n,fm}(T)$ and $M''_{n,fm}(T)$, see Eqs. (3) and (4), as functions of temperature. The zeros of $M'_{n,fm}(T)$ are given by the condition

$$n\omega_0\tau^* = l\pi, \quad \text{(A12)}$$

with l an integer ranging from $n/2 < l \leqslant n$. Similarly, the zeros of $M''_{n,fm}(T)$ coincide with

$$n\omega_0\tau^* = (l + 1/2)\pi. \quad \text{(A13)}$$

Here the integer l ranges from $(n-1)/2 < l \leqslant (2n-1)/2$.

Since we consider the temperature range $T_0 < T < T_C$ close to the Curie temperature T_C, the magnetization $M_0(T)$ and the functions $f_2(T,0)$ and $f_4(T,0)$ are expanded for $M_0(T) \ll 1$. From the Langevin function one obtains

$$M_0^2(T) \simeq \frac{5}{3}\left(\frac{T}{T_C}\right)^2 \varepsilon, \tag{A14}$$

with $\varepsilon = (T_C - T)/T_C$, yielding the mean-field critical exponent $\beta = 1/2$. Similarly, from Eqs. (A3) and (A4) one obtains for $H = 0$

$$f_2(T,0) = \frac{3}{5}\left(\frac{T_C}{T}\right)^2 M_0^2(T), \tag{A15}$$

$$f_4(T,0) = \frac{3}{35}\left(\frac{T_C}{T}\right)^4 M_0^4(T). \tag{A16}$$

Obviously, for $T \lesssim T_C$ the functions $f_2(T,0)$ and $f_4(T,0)$ decrease more rapidly than the magnetization $M_0(T)$, and thus also the effective anisotropies $\mathcal{K}_2(T)$ and $\mathcal{K}_4(T)$ with respect to the Zeeman energy $\propto M_0(T)$. This is the reason why hysteresis loops can be obtained close to T_C also by comparably small magnetic fields. Using these replacements, one obtains from Eq. (A10)

$$\cos(\omega_0 \tau^*) \approx \frac{-2}{\mu_0 \mu H_0}\frac{T_C}{T}\sqrt{\varepsilon}(K_2\alpha_2 + K_4\alpha_4\varepsilon), \tag{A17}$$

with $\alpha_2 = \sqrt{3/5}$ and $\alpha_4 = \sqrt{5/147}$ for classical spins. The zeros T_l' of $M_{n,fm}'(T)$ are given by

$$\cos(\omega_0\tau_c) = \cos(l\pi/n) \equiv c_l' = \frac{-2}{\mu_0\mu H_0}\frac{1}{t_l'}\sqrt{1-t_l'}[K_2\alpha_2 + K_4\alpha_4(1-t_l')], \tag{A18}$$

where $t_l' = T_l'/T_C$. In general, this is a quartic equation for t_l'. For $K_4 = 0$ it reduces to a quadratic equation which can easily be solved,

$$t_l' = 2\left(\frac{K_2\alpha_2}{\mu_0\mu H_0 c_l'}\right)^2\left[\sqrt{1+\left(\frac{\mu_0\mu H_0 c_l'}{K_2\alpha_2}\right)^2} - 1\right]. \tag{A19}$$

Similarly, the zeros $t_l'' = T_l''/T_C$ of $M_{n,fm}''(T)$ are also given by Eqs. (A18) and (A19), if one replaces c_l' by $c_l'' = \cos[\pi(2l+1)/(2n)]$.

*Corresponding author. FAX: +49-30-838-53646. Email address: babgroup@physik.fu-berlin.de

†Present address: Materials Science Department, University of Patras, Gr-26504 Patras, Greece.

[1] H. Stanley, *Introduction to Phase Transitions and Critical Phenomena* (Clarendon Press, Oxford, 1971).

[2] C. Rüdt, P. Poulopoulos, J. Lindner, A. Scherz, H. Wende, K. Baberschke, P. Blomquist, and R. Wäppling, Phys. Rev. B **65**, 220404(R) (2002).

[3] U. Bovensiepen, C. Rüdt, P. Poulopoulos, and K. Baberschke, J. Magn. Magn. Mater. **231**, 65 (2001).

[4] J. Souletie and J.L. Tholence, Solid State Commun. **48**, 407 (1983).

[5] N. Herzum and K. Stierstadt, Intern. J. Magnetism **3**, 39 (1972).

[6] H.P. Oepen, S. Knappmann, and W. Wulfhekel, J. Magn. Magn. Mater. **148**, 90 (1995).

[7] T. Shirane, T. Moriya, T. Bitoh, A. Sawada, H. Aida, and S. Chikazawa, J. Phys. Soc. Jpn. **64**, 951 (1995).

[8] T. Bitoh, T. Shirane, and S. Chikazawa, J. Phys. Soc. Jpn. **62**, 2837 (1993).

[9] T. Bitoh, K. Ohba, M. Takamatsu, T. Shirane, and S. Chikazawa, J. Magn. Magn. Mater. **154**, 59 (1996).

[10] E. Carré and J. Souletie, J. Magn. Magn. Mater. **72**, 29 (1988).

[11] E. Kneller, *Ferromagnetismus* (Springer Verlag, Berlin, 1962).

[12] L.-C. Duda, P. Isberg, S. Mirbt, J.-H. Guo, B. Hjörvarsson, J. Nordgren, and P. Granberg, Phys. Rev. B **54**, 10393 (1996).

[13] P. Isberg, B. Hjörvarsson, R. Wäppling, E.B. Svedberg, and L. Hultman, Vacuum **48**, 483 (1997).

[14] A.N. Anisimov, W. Platow, P. Poulopoulos, W. Wisny, M. Farle, K. Baberschke, B. Hjörvarsson, and R. Wäppling, J. Phys.: Condens. Matter **9**, 10581 (1997).

[15] J. Lindner, C. Rüdt, E. Kosubek, P. Poulopoulos, K. Baberschke, P. Blomquist, R. Wäppling, and D.L. Mills, Phys. Rev. Lett. **88**, 167206 (2002).

[16] U. Stetter, A. Aspelmeier, and K. Baberschke, J. Magn. Magn. Mater. **117**, 183 (1992)

[17] H.-B. Callen and E. Callen, J. Phys. Chem. Solids **27**, 1271 (1966).

[18] H.J. Elmers, J. Hauschild, and U. Gradmann, J. Magn. Magn. Mater. **140–144**, 1559 (1995); Phys. Rev. B **54**, 15 224 (1996).

[19] See, e.g., P. Fröbrich, P.J. Jensen, and P.J. Kuntz, Eur. Phys. J. B **13**, 477 (2000), and references therein.

[20] D. Kerkmann, D. Pescia, and R. Allenspach, Phys. Rev. Lett. **69**, 1289 (1992).

[21] P.J. Jensen, S. Knappmann, W. Wulfhekel, and H.P. Oepen, Phys. Rev. B **67**, 184417 (2003).

[22] The use of quantum spins yields qualitatively the same behavior, with spin-dependent prefactors in the corresponding equations of Appendix A. The main differences between quantum and classical spins appear at low temperatures.

[23] P. Bruno, *Magnetismus von Festkörpern und Grenzflächen* (Forschungszentrum Jülich, 1992), Chap. 24.

[24] See, e.g., P.J. Jensen and K.H. Bennemann, in *Magnetism and Electronic Correlations in Local-Moment Systems: Rare Earth Elements and Compounds*, edited by M. Donath, P.A. Dowben, and W. Nolting (World Scientific, Singapore, 1998), p. 113, and references therein.